Supporting Information

Light-emitting Quantum Dot Transistors: Emission at High Charge Carrier Densities

Julia Schornbaum,[†] Yuriy Zakharko,[†] Martin Held,[†] Stefan Thiemann,[†] Florentina Gannott,[†] and Jana Zaumseil[†‡]*

† Friedrich-Alexander-Universität Erlangen-Nürnberg, Department of Materials Science and Engineering, D-91058 Erlangen, Germany

‡ Universität Heidelberg, Institute for Physical Chemistry, D-69120 Heidelberg, Germany

Email: *zaumseil@uni-heidelberg.de*

1. Methods

Synthesis, fabrication, and characterization

2. Results

A. Photoluminescence (PL) spectra of PbS quantum dot (QD) solutions and films

B. Effect of PbS QD film annealing

C. Current-voltage characteristics of electrolyte-gated field-effect transistors (FETs)

D. Movie of the moving emission zone in an electrolyte-gated PbS QD light-emitting FET

E. Position and width of PbS QD emission zone at different gate voltages

F. FETs with HfO_x dielectric and top gate

G. PbS FETs fabricated with QDs synthesized with $PbCl_2$ and S

H. Gate voltage dependence of PL intensity

I. Calculation of excitation density for lifetime measurements

J. Variation of intensity and PL decay for high electron and hole accumulation levels

K. Radiative exciton lifetime

L. Transient photoluminescence analysis

M. Estimation of PL transients for high electron and hole accumulation levels

N. Influence of the excitation power density on the PL decay

1. Methods

Chemicals. Lead(II) acetate trihydrate ($Pb(COOCH_3)$ x 3 H_2O), 1-octadecene (technical grade 90 %), oleic acid (≥ 99.0 %), **b**is(trimethylsilyl) sulfide (TMS), octane (anhydrous, ≥ 99%), 3-marcaptopropionic acid (MPA; ≥ 99%), poly(vinylidene fluoride-co-hexafluoropropylene) (P(VDF-HFP), $M_w \sim 400$ kg mol^{-1}, $M_n \sim 130$ kg mol^{-1}), hexane, acetone, methanol, and toluene were purchased from Sigma Aldrich, ethanol from Carl Roth GmbH, ionic liquid 1-ethyl-3-methyl-imidazolium-tris(pentafluoroethyl)-trifluorophosphate ([EMIM][FAP], high purity grade, dried in vacuum) from Merck.

Synthesis of PbS. Synthesis of PbS was performed in argon atmosphere using a standard air-free Schlenk-line technique and hot-injection. For a typical synthesis a stock solution of $Pb(oleate)_2$ was prepared by dissolving $Pb(COOCH_3)$ x 3 H_2O (758.6 mg) and oleic acid (6 - 10 mL, depending on QD size) in 1-octadecene (12 ml). The reaction mixture was dried in vacuum at 100 °C for 2 h. It was then heated to 145 °C under moderate argon flow. The sulfur precursor solution (210 µL of TMS in 6 - 10 mL 1-octadecene, prepared in a glove box) was rapidly injected into the $Pb(oleate)_2$ stock solution and the temperature was decreased to 120 °C. The reaction mixture was kept at 120 °C for 10 min and then quenched. The PbS QDs were washed two to three times with hexane/ethanol/acetone by centrifugation at 6000 rpm for 3 min to remove all contaminants. Subsequently, the PbS QDs were transferred into a dry nitrogen glovebox, re-dispersed in 4 mL octane and centrifuged to remove agglomerated and undissolved QDs. The supernatant was kept and used for device fabrication.

Fabrication of PbS LEFETs. Interdigitated source/drain electrodes (channel length L = 5 µm; channel width W = 20 mm) and gold side-electrodes (1.5 × 1.5 mm) were defined

photolithographically using a standard double-layer photoresist (LOR5B/S1813), electron-beam evaporation (2 nm Ti, 30 nm Au) and lift-off process on thin glass substrates (Schott AF32 Eco, thickness 0.3 mm). Before PbS QD deposition the substrates were cleaned with acetone and isopropanol in an ultrasonic bath and subsequently rinsed with deionized water. PbS film formation was carried out in a nitrogen filled glove box. A solution of PbS QDs in octane was passed through a 0.2 μm filter onto the pre-patterned electrodes and spin-coated at 2500 rpm for 10 s. A 1 % v/v solution of MPA in methanol was dropped onto the PbS QD layer to exchange oleic acid ligands. The MPA solution was allowed to remain on the QD layer for 30 s before spinning at 2500 rpm for 10 s. Each layer was then washed with methanol twice to remove any organic residue and then dried for ~ 10 s at 80 °C. The final film was formed by repeating this process several times (layer-by-layer, LBL). Excess PbS QDs outside the interdigitated electrodes were removed with toluene. P(VDF-HFP) was co-dissolved with [EMIM][FAP] in acetone (1:4:14 by mass) and spin-coated on top of the PbS film at 2000 rpm. Excess iongel around the device was removed with acetone. Annealing in nitrogen overnight at ~ 50 °C removed any residual solvent. All devices were encapsulated with a piece of glass and a UV hardening epoxy (Delo Katiobond, LP655 resin) to allow for measurements in air.

Characterization of PbS QDs and LEFETs. UV-Vis absorption spectra of PbS QDs in octane were acquired with a Varian Cary 6000i absorption spectrometer. Transmission electron microscope (TEM) images were recorded with a Philips CM 300 UT operated at 300 kV. Scanning electron microscope (SEM) images of a 5 LBL film on a Si/SiO_2 substrate were acquired with a Zeiss AURIGA microscope at 1 kV. Current-voltage characteristics of the electrolyte-gated transistors were recorded with an Agilent 4155C semiconductor parameter analyzer or a Keithley 2612A source meter. All measurements were performed at room temperature. Electroluminescence (EL) images were recorded with a thermoelectrically

cooled 256 x 360 pixel InGaAs camera (Xenics XEVA-CL-TE3, sensitivity range: 800 - 1600 nm). Photoluminescence (PL) of the LEFETs and EL spectra were obtained with an Acton SpectraPro SP2358 spectrometer (grating 150 lines/mm) and a liquid nitrogen cooled InGaAs line camera (PI Acton OMA V:1024 1.7). For PL measurements a 640 nm laser diode (OBIS, Coherent Europe B.V.) was used. The laser beam was focused onto the substrate through the collecting near-infrared objective (Olympus LCPLN50XIR ×50, NA 0.65 with correction collar for glass thickness). A cold mirror (transmission > 875 nm) and an additional long-pass filter (715 nm) were used to reject visible and scattered laser light. For current-voltage-luminance measurements a calibrated InGaAs photodiode (Thorlabs FGA21-CAL, active area 3.1 mm^2) was placed directly underneath the device (active area ~ 0.1 mm^2) to collect as much of the emitted light as possible. The photocurrent was recorded at 0 V bias. Calculations of the external quantum efficiency took the observed electroluminescence spectrum and wavelength dependent sensitivity of the photodiode into account. Given the expected losses due to absorption, waveguiding and emission in all directions (not just toward the photodiode), the obtained EQE is a lower boundary for the overall efficiency.

PL lifetime measurements. Samples were illuminated through the substrate glass with a pulsed (< 60 ps, 1 MHz or 10 MHz) diode laser at 785 nm (Alphalas GmbH) focused with a ×100 near-IR 0.8 N.A. objective. Emitted photons were collected with the same objective and directly detected with an InGaAs/InP single-photon avalanche diode (Micro Photon Devices, Italy). Statistics of the arrival times of the photons were acquired with time-correlated single-photon counting module (Picoharp 300, Picoquant GmbH) at time bin 32 ps. The instrument response function FWHM ~ 100 ps was estimated from the fast photoluminescence decay of a low bandgap diketopyrrolopyrrole copolymer (DPPT-BT). Excitation photon fluxes per pulse were 0.088 x 10^{15} cm^{-2} and 2.096 x 10^{15} cm^{-2}.

Obtained PL decay curves were fitted to a mono-exponential function or reconvoluted to a tri-exponential function with Symphotime 64 (Picoquant) taking into account the measured IRF.

PL Quantum Yield. For PL quantum yield (QY) measurements a 785 nm laser beam was directed through the entrance port of an integrating sphere (LabSphere, Spectralon coating). Quantum dot solutions enclosed in quartz cuvettes and thin film samples, respectively, were mounted on a PTFE sample holder in the center of the sphere. Quantum yield measurements were performed according to DeMello *et al.*[1] The laser beam was directed either onto the sample (direct excitation) or on the wall of the integrating sphere (indirect excitation). The scattered laser light and PL signal were fiber-coupled to the Acton SpectraPro SP2358 spectrometer. Emission spectra were compared to PL spectra measured outside the sphere to account for re-absorption/re-emission effects in the integrating sphere.[2] All spectra were corrected for the spectral response of the systems with a calibrated tungsten halogen lamp.

2. Results

A. Photoluminescence (PL) spectra of PbS quantum dot (QD) solutions and films

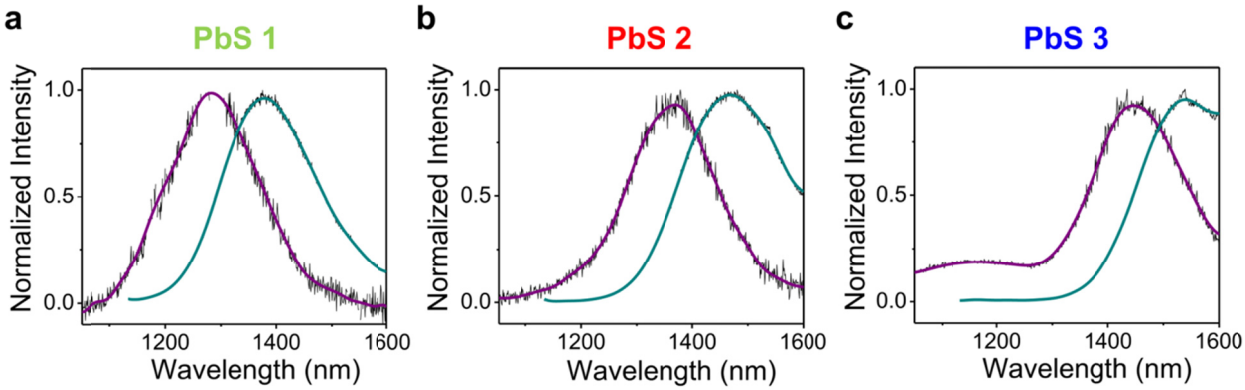

Figure S1. PL spectra of PbS QD solutions (purple) and 5 LBL thin-films (turquois) of (a) PbS 1, (b) PbS 2, and (c) PbS 3. The red-shift of the PL signal is due to the ligand exchange from oleic acid to 3-mercaptopropionic acid (MPA).

B. Effect of PbS QD film annealing

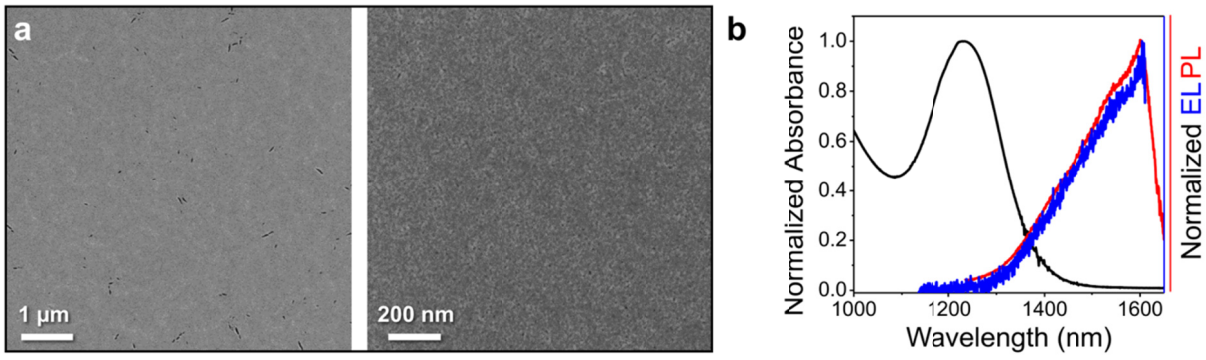

Figure S2. (a) Top view scanning electron microscopy images of a 6 LBL thin PbS QD film annealed at 120 °C for 30 min. (b) Normalized absorption spectrum of PbS QD solution (black) and PL (red) and electroluminescence (EL) (blue) spectra of an annealed 6 LBL thin film of the same QDs (PbS 1). Annealing removes the cracks resulting in smooth thin films but also red-shifts PL and EL spectra beyond the detector range (cut-off at 1600 nm).

C. Current-voltage characteristics of electrolyte-gated field-effect transistors (FETs)

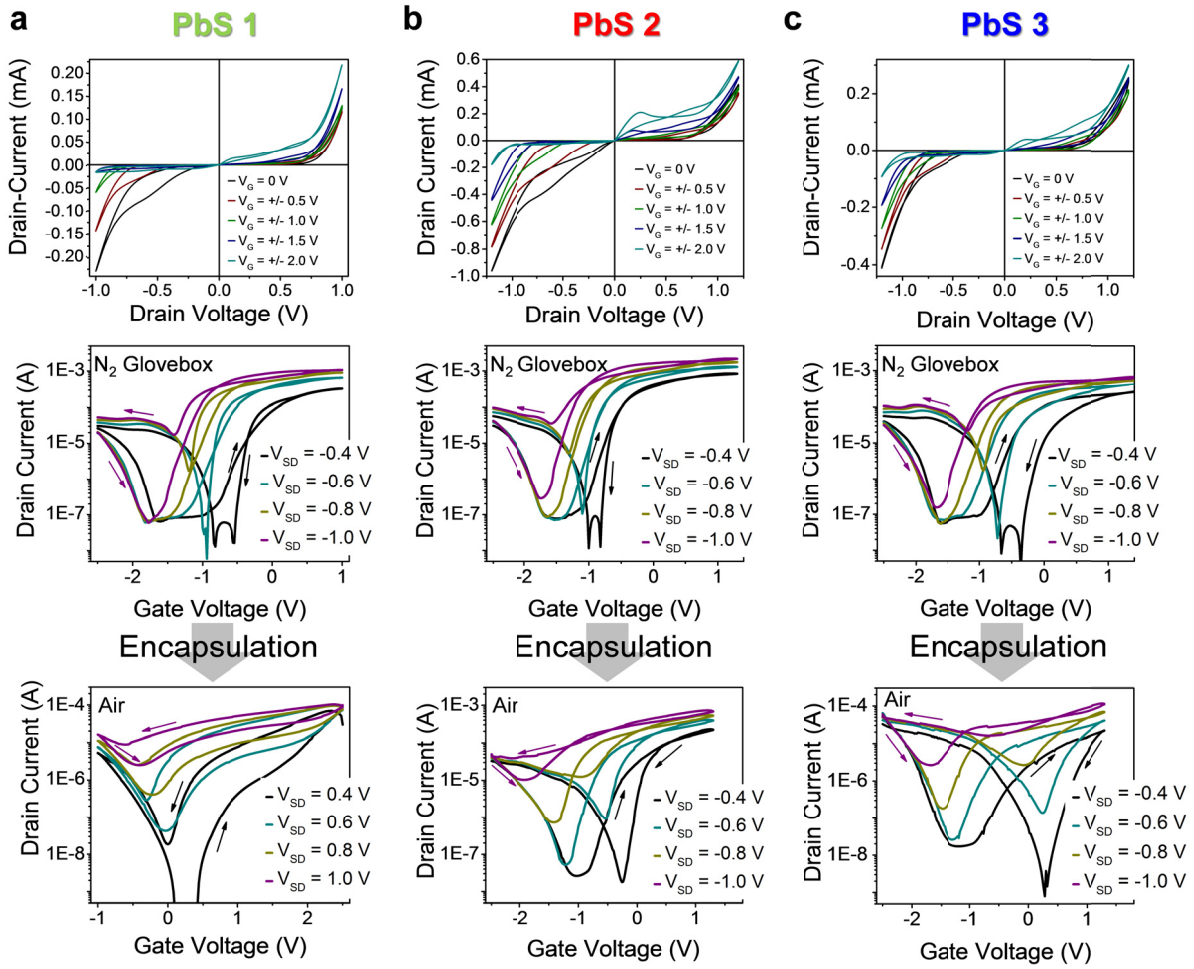

Figure S3. Ambipolar output and transfer characteristics of FETs fabricated with (a) PbS 1, (b) PbS 2, and (c) PbS 3 quantum dots measured in a nitrogen-filled glovebox before encapsulation (top rows) and in air after encapsulation (bottom row). Encapsulation protects PbS QDs against oxidation and devices retain their ambipolar behavior in air.

D. Movie of the moving emission zone in an electrolyte-gated PbS QD light-emitting FET

Near-infrared movie (wavelengths 800 - 1600 nm) of the recombination and emission zone from a PbS QD FET (electrolyte-gated, PbS 3 QDs) for a gate voltage sweep (forward and reverse from +1.3 V to -2.5 V) and constant source-drain voltage (V_{SD} = -1.2 V); integration time per frame: 5 s; movie with 10 frames per second.

E. Position and width of PbS QD emission zone at different gate voltages

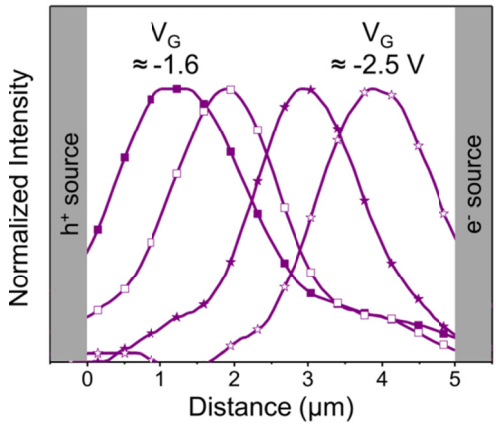

Figure S4. Position (distance from hole injecting electrode) of emission zone of a PbS (QDs 2) FET (channel length L = 5 µm, channel width W = 20 mm, integration time: 5 s) at different gate voltages and constant source-drain voltage (V_{SD} = -1.0 V) (see Figure 2). The apparent full width at half maximum (FWHM) of about 2 µm is partially caused by the limited resolution of the optical setup in the near-infrared.

F. FETs with HfO_x dielectric and top gate

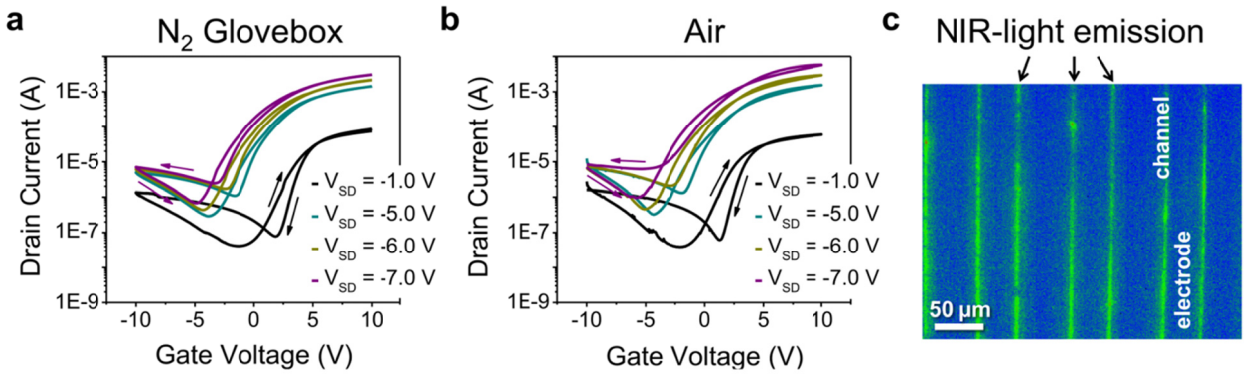

Figure S5. Ambipolar transfer characteristics of a PbS FET (PbS 1 QDs; channel length L = 5 µm; channel width W = 20 mm) with 50 nm HfO_x as the dielectric (deposited via atomic layer deposition) and a conventional evaporated silver top-gate measured in (a) a nitrogen-filled glovebox and (b) in air without encapsulation. The air stability can be attributed to the HfO_x infilling of PbS QD solids and therefore protection against oxidation.[3] However, we were not able to achieve high hole currents with this transistor geometry and (c) electroluminescence was very weak and hardly detectable (false-color near-infrared image at V_G = 9 V and V_{SD} = -6 V, integration time: 5 s, wavelength range: 800 - 1600 nm).

G. PbS FETs fabricated with QDs synthesized with $PbCl_2$ and S

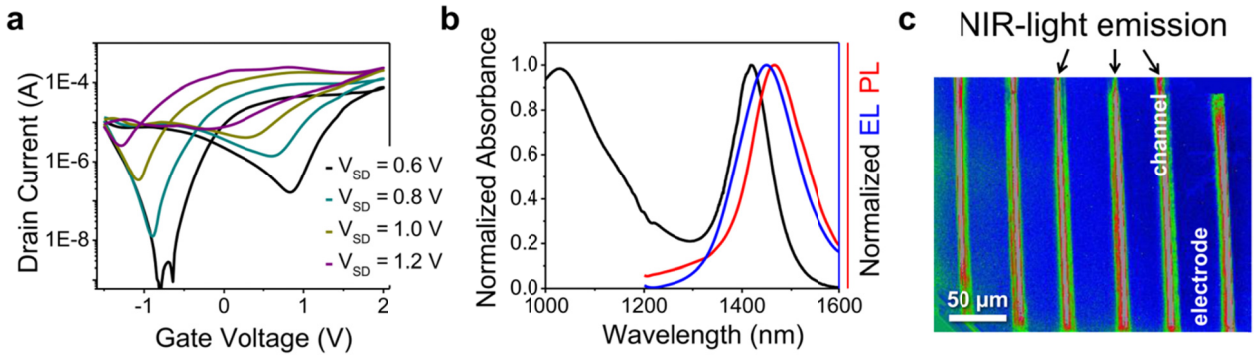

Figure S6. (a) Ambipolar transfer characteristics of a PbS FET fabricated with PbS QDs synthesized with $PbCl_2$ and elemental sulfur according to Weidman *et al.*[4] Films were annealed at 120 °C for 30 min. Hole currents were low and could not be increased by using higher concentrated PbS QD dispersions or more layers. (b) Normalized absorption spectrum of PbS solution (black) and EL (blue) and PL (red) spectra of the electrolyte-gated transistor fabricated with the same QDs. Spectra show very narrow peaks and almost no Stokes shift. PbS QDs are very stable against annealing and apparently no loss of ligands or/and sintering of the QDs takes place. However, currents remain low and the emission zone does not move through the channel by applying different gate voltages, but remains at the hole injecting electrode: (c) False-color near-infrared image (wavelengths 800 - 1600 nm, integration time: 30 s) of the recombination and emission zone (V_G = 2 V, V_{SD} = -1 V).

H. Gate voltage dependence of PL intensity

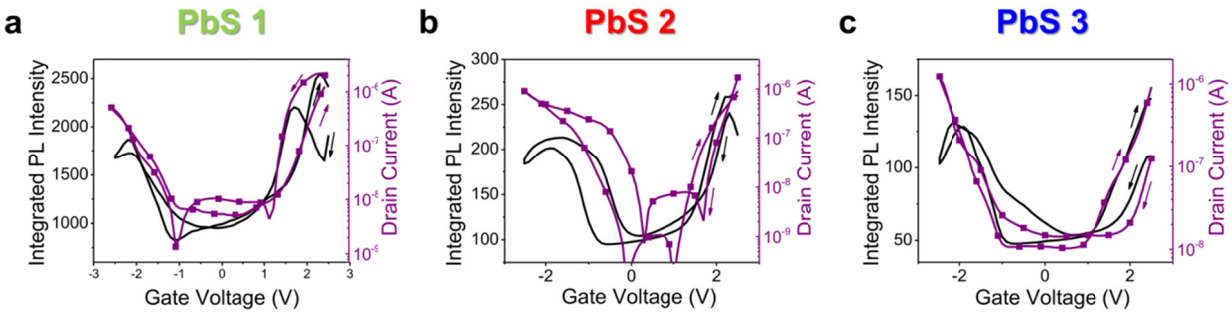

Figure S7. Integrated PL intensity from the channel region at different gate voltages under constant laser excitation (λ_{exc} = 640 nm, ~ 10 mW/μm^2) and a very small constant V_{SD} = -0.01 V for (a) PbS 1, (b) PbS 2, and (c) PbS 3. Integrated PL intensity follows charge accumulation. It shows a sharp increase in intensity at the threshold for both, electron and hole transport.

I. Calculation of excitation density for lifetime measurements

The excitation density can be defined as the number of absorbed photons per quantum dot per pulse:

$$N = N_{ph}\sigma \quad (1)$$

, where N_{ph} is the photon flux per pulse and σ is the absorption cross section of a quantum dot.

The average photon flux is calculated according to the following equation:

$$N_{ph} = \frac{P_{av}}{f}\frac{\lambda}{hc}\frac{1}{\pi r^2} \quad (2)$$

, where P_{av} is the average laser power, f is the laser repetition rate, λ is the excitation wavelength, h is the Planck´s constant, c is the speed of light and r is the radius of the diffraction limited focal spot (accounting for objective NA = 0.8).

For the two average laser powers we used in this work (630 nW and 15 μW), the photon fluxes per pulse are equal to:

$N_{ph1} = 0.088 \times 10^{15} cm^{-2}$ and $N_{ph2} = 2.096 \times 10^{15} cm^{-2}$

The absorption cross section can be calculated using the following formula:[5]

$$\sigma_1 = \frac{4\pi}{n\lambda}\left|f_{lf}\right|^2 n_{PbS} k_{PbS} \left(\frac{4}{3}\pi r_{QD}^3\right) \quad (3)$$

, where λ is the photon wavelength in vacuum, n is the refractive index of the environment (~1.5 accounting for the glass substrate and the iongel), n_{PbS} and k_{PbS} are the refractive index and the extinction coefficient of bulk lead sulfide at λ, r_{QD} is the radius of the quantum dot. The local field correction factor is calculated according to:

$$\left|f_{lf}\right|^2 = \frac{9n^4}{(n_{PbS}^2 - k_{PbS}^2 + 2n^2)^2 + 4n_{PbS}^2 k_{PbS}^2} \approx 0.066$$

This yields the following absorption cross sections of PbS 1, PbS 2, and PbS 3:

$\sigma_{1\_PbS1} = 1.3 \times 10^{-15} cm^2$, $\sigma_{1\_PbS2} = 1.59 \times 10^{-15} cm^2$ and $\sigma_{1\_PbS3} = 2.17 \times 10^{-15} cm^2$

This method (Equation 3) is usually used for diluted samples and single QD studies, and thus in our case of closed packed QD solid films the local field correction factor and the corresponding absorption cross section may deviate.

Alternatively, the effective absorption cross section of the QDs in our thin solid films can be defined as:[6]

$$\sigma_2 = \frac{1 - e^{-\alpha L}}{cL} \quad (4)$$

, where L is the thickness of the QD film, c is the concentration of the QDs and α is the absorption coefficient:

$$\alpha = \frac{4\pi k_{PbS}}{\lambda} \approx 16 \times 10^4\ cm^{-1}$$

This yields following absorption cross sections of PbS 1, PbS 2, and PbS 3:

$\sigma_{2\_PbS1} = 1.76 \times 10^{-15} cm^2$, $\sigma_{2\_PbS2} = 2.15 \times 10^{-15} cm^2$ and $\sigma_{2\_PbS3} = 2.93 \times 10^{-15} cm^2$

Combining the obtained excitation photon fluxes per pulse per QD and the absorption cross section into Equation 1, we can verify that an average number of absorbed photons per QD per pulse is less than one ($N \leq 1$) for the laser power (630 nW) used in the main text.

J. Variation of intensity and PL decay for high electron and hole accumulation levels

The average photoluminescence lifetime in the main text is defined as:[7]

$$\tau = \int_0^\infty \frac{PL(t)}{A_0} dt \quad (5)$$

, where A_0 is the intensity of the decay curve $PL(t)$ at time zero.

This quantity corresponds to the average arrival/detection time of the photons. Strictly speaking it should be corrected for the IRF, but for average lifetimes longer than the IRF the deviations are insignificant.

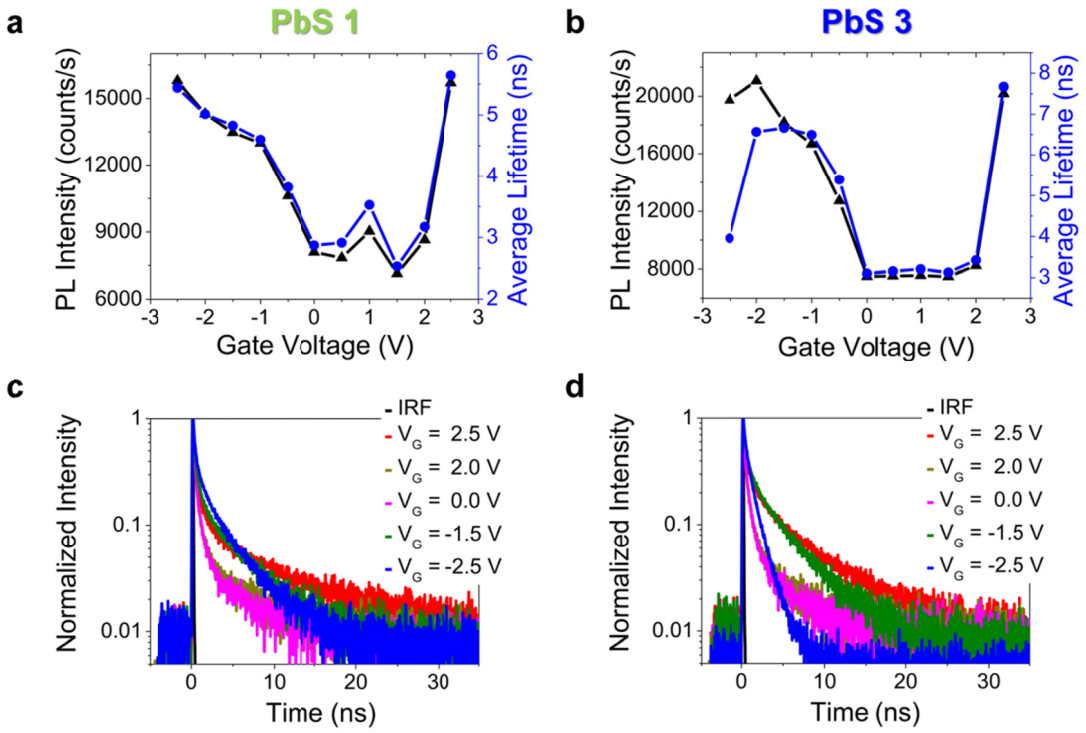

Figure S8. Integrated PL intensity (black triangles) and average emission lifetime (blue circles) at different doping levels for (a) PbS 1 and (b) PbS 3 samples; and (c), (d) corresponding normalized PL decays for selected gate voltages.

K. Radiative exciton lifetime

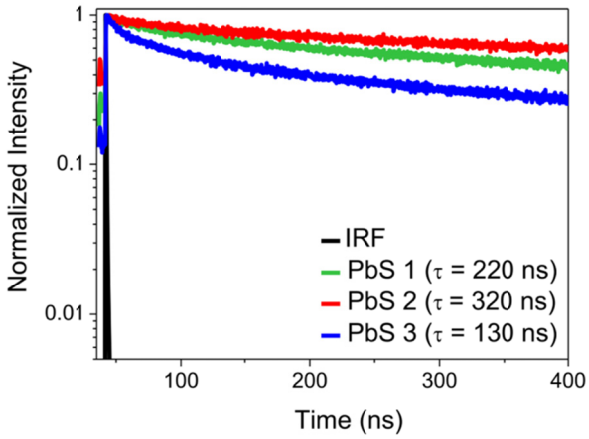

Figure S9. Normalized PL decays for all three PbS QDs in solution. The corresponding average decay lifetimes are τ (PbS 1) = 220 ns, τ (PbS 2) = 320 ns, and τ (PbS 3) = 130 ns.

Photoluminescence quantum yield is defined as:

$$QY = \frac{1/\tau_r}{1/\tau_m} = \frac{\tau_m}{\tau_r} \Rightarrow \tau_r = \frac{\tau_m}{QY} \quad (6)$$

, where τ_r and τ_m are radiative and measured lifetimes respectively.

This yields the following exciton radiative lifetimes of PbS 1, PbS 2, and PbS 3 quantum dots:

$$\tau_{r1} = \frac{220\ \text{ns}}{0.12} = 1.83\ \mu\text{s}\ ;\ \tau_{r2} = \frac{320\ \text{ns}}{0.11} = 2.91\ \mu\text{s}\ \text{ and }\ \tau_{r3} = \frac{130\ \text{ns}}{0.13} = 1\ \mu\text{s}$$

The calculated radiative lifetimes of excitons are in agreement with previous reports.[4,8]

L. Transient photoluminescence analysis

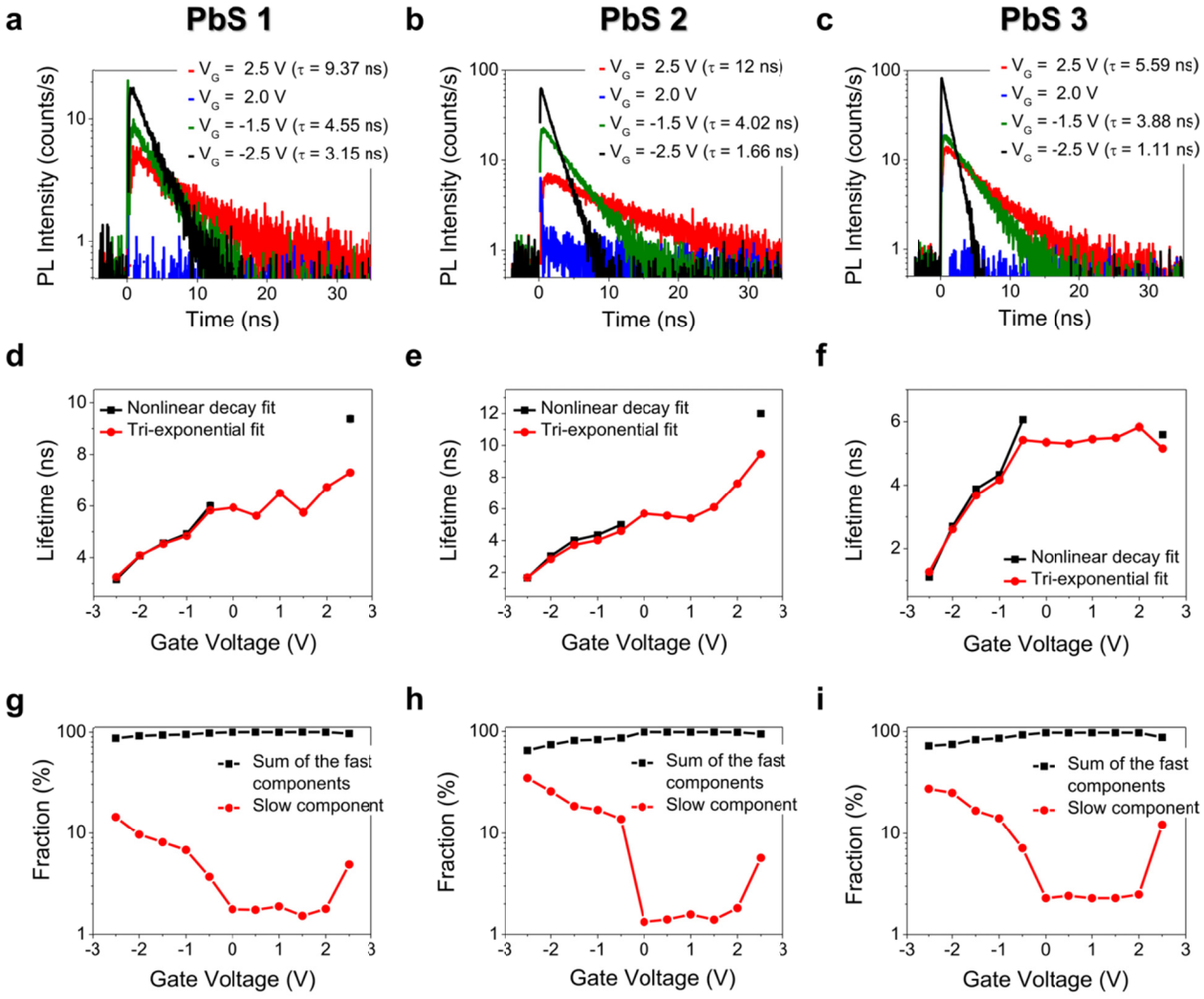

Figure S10. Nonlinear PL transients of (a) PbS 1, (b) PbS 2 and (c) PbS 3 for the selected gate voltages extracted from the PL decay curves (Figure 4c and Figure S8c and S8d by subtraction of the PL decay at $V_G = 0$ V). (d), (e), (f), Corresponding lifetime dependencies of the slow decay component estimated by the mono-exponential fit (black squares) compared to the tri-exponential fit (red circles) of the PL decays (Figure 4c and Figure S8c and S8d). (g), (h), (i), Relative contributions of the sum of the first two fast components (with 120 and 600 ps lifetime) (black squares) and the slow decay component (red circles) to the total light emission as a function of gate voltage (extracted from the tri-exponential fit).

Accounting for the IRF, PL curves can be reconvoluted to a tri-exponential function:

$$PL_{measured}(t) = IRF \otimes (A_1 e^{-t/\tau_1} + A_2 e^{-t/\tau_2} + A_3 e^{-t/\tau_3}) \quad (7)$$

, where coefficients A_1, A_2, A_3 were renormalized:

$$N_{1,2,3} = \frac{A_{1,2,3}}{A_1 + A_2 + A_3} \quad (8)$$

in order to extract relative contribution of the QDs emitting with different lifetimes ($N_1 + N_2 + N_3 = 1$ (*i.e.* 100%)).

We highlight that a tri-exponential fit can give arbitrary dependencies of the amplitudes and lifetimes representing QDs with different radiative and non-radiative decay rates and including charge transfer between them. Therefore, in order to numerically impose the dependence for QDs with different doping levels and taking into account our previous consideration, the following fitting restrictions were applied: a) lifetime of the two fast components remain constants (120 ps and 600 ps, preliminary fitted for V_G = 0 V), while their coefficients (reflecting the fraction of QDs with a particular decay time constant) are fitted, and b) both amplitude and lifetime of the slow component are fitted. These restrictions resemble a nonlinear transient method used to extract lifetimes of the slow decay component, after subtraction of the fast decay components.

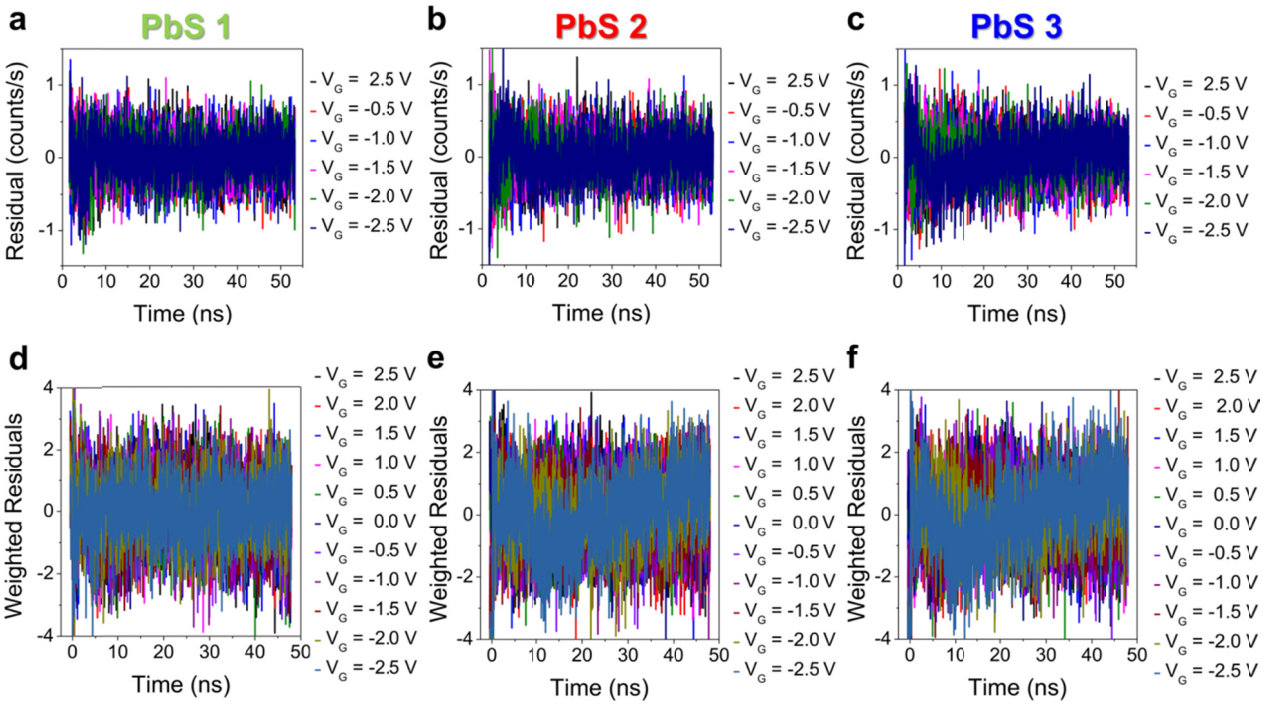

Figure S11. Residuals of the mono-exponential fits of (a) PbS 1, (b) PbS 2, and (c) PbS 3 nonlinear PL transients (Figure S10a-c); and (d), (e), (f) weighted residuals ($R(t) = \frac{(Decay(t) - Fit(t))}{\sqrt{Decay(t)}}$) of the tri-exponential reconvolution fit for the same QDs of the PL decays in Figure 4c and Figure S8c and S8d.

M. Estimation of PL transients for high electron and hole accumulation levels

The three populations of QDs with electronic transitions illustrated in the middle column of Figure 5 (0 V < V_G < 2 V), which are responsible for the observed intensity and lifetime changes, can be described by the following tri-exponential function:

$$PL_{V_G=0\,V}(t) = (N_1 + N_3)e^{-t(\gamma_{rX0}+\gamma_{nrX0}+\gamma_{nr})} + N_2 e^{-t(\gamma_{rX0}+\gamma_{nrX0})} \quad (9)$$

, where N_1 and N_3 correspond to the particles with mostly hole or electron traps, and N_2 represents QDs with almost none of them active. The lifetime of each component is a function of the radiative decay rate of excitons γ_{rX0}, the intrinsic nonradiative decay rate of excitons γ_{nrX0}, and the effective trapping rate of charge carriers γ_{nr} (previously fitted by two fast components in tri-exponential PL decay fits).

In case of hole or electron injection at high gate voltages (see Figure 5, left (V_G > 2 V) and right (V_G < 0 V) columns), Equation 9 transforms into:

$$PL_{V_G=2.5V} = (N_1 + N_3 - \Delta N)e^{-t(\gamma_{rX-}+\gamma_{nrX-}+\gamma_{nr})} + (N_2 + \Delta N)e^{-t(\gamma_{rX-}+\gamma_{nrX-})} \quad (10a)$$

$$PL_{V_G=-2.5V} = (N_1 + N_3 - \Delta N)e^{-t(\gamma_{rX+}+\gamma_{nrX+}+\gamma_{nr})} + (N_2 + \Delta N)e^{-t(\gamma_{rX+}+\gamma_{nrX+})} \quad (10b)$$

, with the radiative and nonradiative rate of excitons replaced with those for trions ($y_{rX-}, y_{rX+}, y_{nrX-}, y_{nrX+}$). ΔN corresponds to the increase of the fraction of QDs with recombination centers deactivated.

By subtracting Equation 9 from the Equations 10a and 10b we obtain functions corresponding to the nonlinear PL (NPL) transient signal used to estimate the decay time of the slow decaying component associated with trion emission (Figure S10a-c):

$$NPL_{V_G=2.5V}(t) = \Delta N[e^{-t(\gamma_{rX-}+\gamma_{nrX-})} + \frac{N_2}{\Delta N}(e^{-t(\gamma_{rX-}+\gamma_{nrX-})} - e^{-t(\gamma_{rX0}+\gamma_{nrX0})}) - e^{-t(\gamma_{rX-}+\gamma_{nrX-}+\gamma_{nr})}] \quad (11a)$$

$$NPL_{V_G=-2.5V}(t) = \Delta N[e^{-t(\gamma_{rX+}+\gamma_{nrX+})} + \frac{N_2}{\Delta N}(e^{-t(\gamma_{rX+}+\gamma_{nrX+})} - e^{-t(\gamma_{rX0}+\gamma_{nrX0})}) - e^{-t(\gamma_{rX+}+\gamma_{nrX+}+\gamma_{nr})}] \quad (11b)$$

Here, at sufficiently long times (> 1 ns) the fast decay exponent (last component) is relatively small compared to the first two components, and thus can be discarded. Additionally, at high charge accumulation levels $\Delta N > N_2$, only the first component, which corresponds to the trion emission, is dominant. These considerations justify the assignment of the obtained lifetime values to the lifetime of trions.

N. Influence of the excitation power density on the PL decay

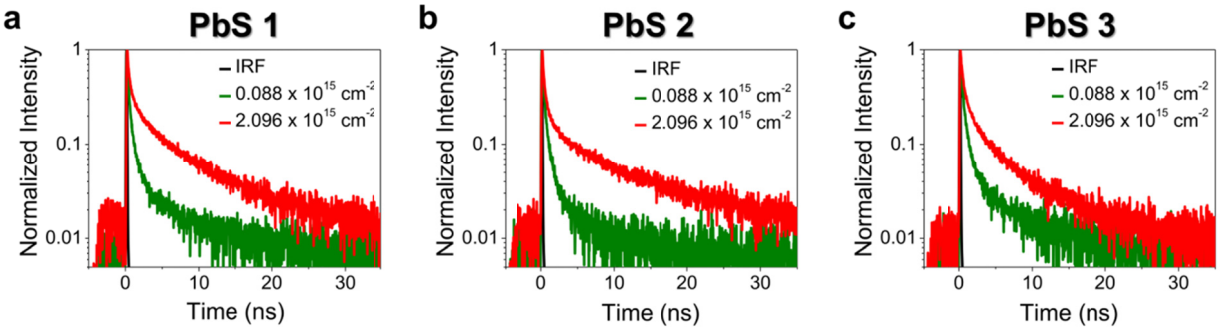

Figure S12. Normalized PL decays of (a) PbS 1, (b) PbS 2, and (c) PbS 3 at two different excitation photon densities per pulse (green and red). With increase of the excitation power, a similar slow decay component appears as in the case of electron or hole accumulation regimes by applying a gate voltage (Figures 4c and S8c and S8d). This effect can be understood as the saturation of trap states, and thus, their effective deactivation.

References

(1) de Mello, J. C.; Wittmann, H. F.; Friend, R. H. *Adv. Mater.* **1997**, *9*, 230-232.

(2) Ahn, T.-S.; Al-Kaysi, R. O.; Müller, A. M.; Wentz, K. M.; Bardeen, C. J. *Rev. Sci. Instrum.* **2007**, *78*, 086105.

(3) Liu, Y.; Gibbs, M.; Perkins, C. L.; Tolentino, J.; Zarghami, M. H.; Bustamante, J.; Law, M. *Nano Lett.* **2011**, *11*, 5349-5355.

(4) Weidman, M. C.; Beck, M. E.; Hoffman, R. S.; Prins, F.; Tisdale, W. A. *ACS Nano* **2014**, *8*, 6363-6371.

(5) Ricard, D.; Ghanassi, M.; Schanne-Klein, M. C. *Opt. Commun.* **1994**, *108*, 311-318.

(6) Trinh, M. T.; Houtepen, A. J.; Schins, J. M.; Hanrath, T.; Piris, J.; Knulst, W.; Goossens, A. P. L. M.; Siebbeles, L. D. A. *Nano Lett.* **2008**, *8*, 1713-1718.

(7) Saba, M.; Aresti, M.; Quochi, F.; Marceddu, M.; Loi, M. A.; Huang, J.; Talapin, D. V.; Mura, A.; Bongiovanni, G. *ACS Nano* **2013**, *7*, 229-238.

(8) Warner, J. W.; Thomsen, E.; Watt, A. R.; Heckenberg, N. R.; Rubinsztein-Dunlop, H. *Nanotechnology* **2005**, *16*, 175-179.